Polymer Chemistry

Accepted Manuscript

ROYAL SOCIETY OF CHEMISTRY

www.rsc.org/polymers

Photoredox Catalysis using a new Iridium Complex As an Efficient Toolbox for Radical, Cationic and Controlled Polymerizations under Soft Blue to Green Lights.

Sofia Telitel [a], Frederic Dumur [b], Siham Telitel [a], Olivier Soppera [a], Marc Lepeltier [c], Yohann Guillaneuf [b], Julien Poly [a], Fabrice Morlet-Savary [a], Philippe Fioux,[a] Jean-Pierre Fouassier[d], Didier Gigmes [b*], Jacques Lalevée [a*]

a) Institut de Science des Matériaux de Mulhouse, UMR CNRS-UHA 7361, 15 rue Jean Starcky, 68057 Mulhouse Cedex, France.
b) Aix-Marseille Université, CNRS, Institut de Chimie Radicalaire, UMR 7273, F-13397 Marseille, France.
c) Institut Lavoisier de Versailles ILV, UMR 8180 CNRS, Université de Versailles Saint-Quentin en Yvelines, 45 avenue des Etats-Unis, 78035 Versailles Cedex – France.
d) ENSCMu-UHA, 3 rue Alfred Werner, 68200 Mulhouse, France.
*Corresponding author: jacques.lalevee@uha.fr; didier.gigmes@univ-amu.fr

Abstract:

A new iridium complex (**nIr**) was designed and investigated as a photoinitiator catalyst for radical and cationic polymerizations upon very soft irradiations (lights ranging from 457 to 532 nm). A ring-opening polymerization (ROP) of an epoxy monomer was easily promoted through the interaction between **nIr** and an iodonium salt (Iod) upon light. The addition of N-vinylcarbazole (NVK) enhances the performance. In radical polymerization, **nIr** can be efficient in combination with phenacyl bromide (PBr) and optionally an amine: these photoinitiating systems work according to an original oxidative cycle and a regeneration of **nIr** is observed. A control of the methyl methacrylate polymerization (conducted under a 462 nm light) with 1.2-1.6 polydispersity indexes was displayed. Surface modifications by direct laser write was also easily carried out for the first time through surface re-initiation experiments, i.e. the dormant species being reactivated by light in the presence of **nIr**; the polymer surfaces were analyzed by XPS. The chemical mechanisms were examined through laser flash photolysis, NMR, ESR and size exclusion chromatography experiments.

Keywords: Photoredox Catalysis, photoinitiator, Iridium complexes, LED, radical Photopolymerization, cationic Photopolymerization, living Photopolymerization, surface modification.

Introduction:

The use of metal based complexes and metal free organic compounds as photocatalysts in organic chemistry is now well-documented.[1-5] In this field, the photoredox catalysis has been found to be a very elegant approach for the generation of radicals upon very soft conditions (sunlight, fluorescences bulbs, LED bulbs…).[1-5] Although organometallic complexes have been relatively widely proposed in the photopolymerization area,[6-7] this photoredox catalysis has been only recently introduced in the photoinduced free radical polymerization FRP of acrylates and cationic polymerization CP (or free radical promoted cationic photopolymerization FRPCP) of epoxides and vinyl ethers. In that case, the photoinitiating system (PIS) is based on a photoinitiator catalyst (PIC) in combination with various additives i.e. oxidation and reduction agents allowing catalytic cycles and regeneration of the PIC. Ruthenium or iridium complexes as well as metal-free organic compounds have been shown to act as efficient PICs in suitable PISs (containing diphenyliodonium hexafluorophosphate (Iod/silane) or phenacyl bromide (PBr)/*N*-methyldiethanolamine (MDEA) and working through oxidation or reduction cycles) to initiate such reactions using very soft irradiation conditions [8,9,10]; see also a recent review in [11] and references therein.

On another side, the control of polymerization reactions that is usually thermally achieved through atom transfer radical polymerization (ATRP), nitroxide mediated polymerization (NMP) and reversible addition fragmentation chain transfer polymerization (RAFT)[12] has been extended in the last years to a control through a photochemical activation.[13-22] In this area, copper [13-15] and iridium [16-19] complexes are largely used as photocatalysts for a successful access to complex architectures or polymer functionalization under exposure to household fluorescent tubes,[16a] mercury lamp,[18] or LEDs (420 or 435 nm) [17,19] delivering near UV or/and visible lights;[16a,13,19] even sunlight can be used.[13] The most widely encountered Ir complex in controlled or living radical polymerization but also in mediated atom transfer radical addition (ATRA) is tris[2-phenylpyridinato-C^2,*N*] iridium(III) [$Ir(ppy)_3$]. [16-19]

The search for other iridium complexes is driven by the requirement to have systems exhibiting better light absorption properties and, if possible, an ever enhanced reactivity. Indeed, $Ir(ppy)_3$ is characterized by a maximum absorption wavelength in the UV range (~370

nm) and its visible light absorption remain rather moderated. We have already checked the ability of various Ir complex derivatives for the CP of an epoxide (Ir complex/Iod/silane as PIS) and the FRP of acrylates (Ir complex/PBr/MDEA as PIS).[23-24]

In the present paper, we propose a new iridium complex ($Ir(btp)_2(tmd)$ also called **nIr** in Scheme 1) as a novel PIC with enhanced efficiency under visible light (laser diodes at 457 and 532 nm, LED at 462 nm and household halogen lamp) for i) CP/FRPCP (when combined with Iod and eventually *N*-vinylcarbazole NVK), ii) FRP (PBr and optionally MDEA being added), iii) controlled/living radical polymerization and iv) polymer surface modification, including micropatterning by laser direct writing. According to the novel ligands that have been introduced, a change in the reactivity can be expected. The chemical mechanisms are investigated by electron spin resonance (ESR), laser flash photolysis, size exclusion chromatography, absorption and luminescence experiments. Shifting the absorption spectrum of such advanced photoinitiating systems towards visible wavelengths is bringing specific advantages such as recourse to low cost and low-energy light sources or even solar light and laser diodes for direct write.

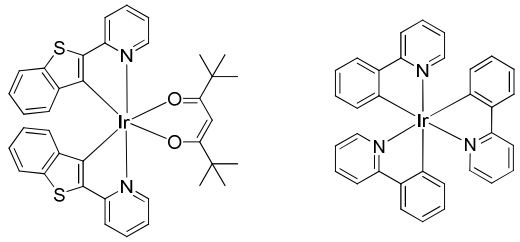

nIr $Ir(ppy)_3$

Scheme 1.

Experimental Section

i) Synthesis of $Ir(btp)_2(tmd)$:

^1H and ^{13}C NMR spectra were recorded at room temperature in 5 mm o.d. tubes on a Bruker Avance 300 spectrometer equipped with a QNP probe head : ^1H (300 MHz) and ^{13}C (75 MHz). The ^1H chemical shifts were referenced to the solvent peak: $CDCl_3$ (7.26 ppm), and the ^{13}C chemical shifts were referenced to the solvent peak: $CDCl_3$ (77.0 ppm). / All

starting materials and solvents were purchased from Aldrich or Alfa Aesar and used as supplied commercially. The synthetic procedure is summarized in Schemes 2-3.

$Ir(ppy)_2Cl_2Ir(ppy)_2$. To a solution of 2-phenylpyridine (2.29 g, 14.8 mmol) in a 2-ethoxyethanol / water (75 : 25, 50 mL) mixture was added $IrCl_3.3H_2O$ (1.45 g, 4.23 mmol). The reaction was stirred at reflux for 24h. Then, water (50 mL) was added and the product was filtered, washed, with ethanol and diethyl ether. The product was then isolated as a yellow powder (2.02 g, 89 %). ^{1}H NMR (300 MHz, $CDCl_3$, ppm): 9.25 (d, ^3J = 5.4 Hz, 4H), 7.88 (d, ^3J = 8.1 Hz, 4H), 7.75 (dt, ^3J = 7.2 Hz, ^4J = 1.5 Hz, 4H), 7.50 (dd, ^3J = 7.8 Hz, ^4J = 1.2 Hz, 4H), 6.77 (m, 8H), 6.57 (dt, ^3J = 7.8 Hz, ^4J = 0.9 Hz, 4H), 5.94 (d, ^3J = 7.5 Hz, 4H).

fac-$Ir(ppy)_3$. To a suspension of the dimer *$Ir(ppy)_2Cl_2Ir(ppy)_2$* (200 mg, 0.187 mmol) in glycerol (30 mL) was added 2-phenylpyridine (87 mg, 0.56 mmol) and sodium carbonate (200 mg, 1.87 mmol). The reaction mixture was stirred at reflux for 24h. Then, water (50 mL) was added and the product was filtered, washed, with ethanol and diethyl ether. The product was purified by chromatography on silica gel and was isolated as a yellow powder (140 mg, 57 %). ^{1}H NMR (300 MHz, $CDCl_3$, ppm): 7.89 (d, ^3J = 8.4 Hz, 3H), 7.67 (d, ^3J = 7.2 Hz, 3H), 7.59 (dt, ^3J = 8.1 Hz, ^4J = 1.8 Hz, 3H), 7.54 (d, ^3J = 5.7 Hz, 3H), 6.90 (m, 12H). MS (ESI) Calcd for $C_{33}H_{24}IrN_3$ 655.1599; Found 655.1633 $[M]^+$.

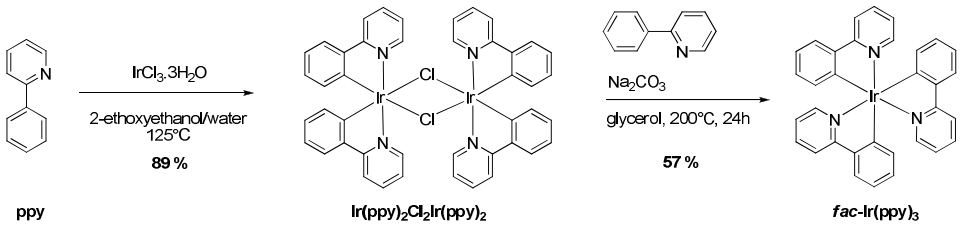

Scheme 2.

2-(2'-benzothienyl)pyridine (btp) was prepared following the literature procedure and obtained in a similar yield.[25a] Cyclometalated iridium dimer $Ir_2(btp)_4\mu$-Cl_2 was synthesized under an inert atmosphere according to the Nonoyama route by refluxing $IrCl_3.3H_2O$ with 2–2.5 equiv. of cyclometalating ligand in a 3:1 mixture of 2-ethoxyethanol and water, using a detailed procedure recently reported.[25b]

$Ir(btp)_2Cl_2Ir(btp)_2$. To a solution of 2-(2'-benzothienyl)pyridine (0.65 g, 3.08 mmol) in a mixture 2-ethoxyethanol / water (75 : 25, 50 mL) was added $IrCl_3.3H_2O$ (0.38 g, 1.10

mmol). The reaction was stirred at reflux for 24h. Then, water (50 mL) was added and the product was filtered, washed, with ethanol and diethyl ether. The product was then isolated as a red powder (0.70 g, 98 %).

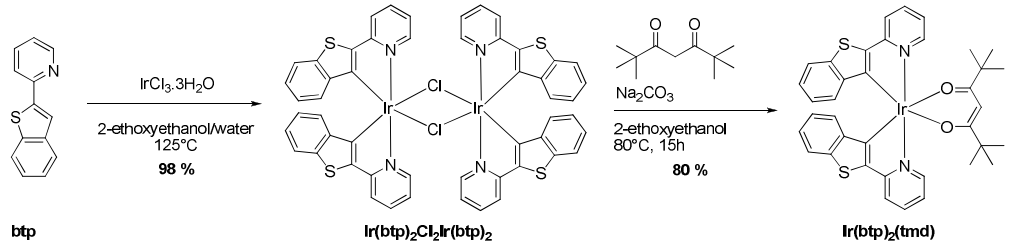

Scheme 3.

Ir(btp)$_2$(tmd) also called **nIr**. To a suspension of the dimer *Ir(btp)$_2$Cl$_2$Ir(btp)$_2$* (200 mg, 1.54 mmol) in 2-ethoxyethanol (30 mL) was added 2,2,6,6-tetramethyl-3,5-heptanedione (86 mg, 4.63 mmol) and sodium carbonate (165 mg, 1.56 mmol). The reaction mixture was stirred at reflux for 15h. Then, water (50 mL) was added and the product was filtered, washed, with ethanol and diethyl ether. The product was purified by chromatography on silica gel and was isolated as a red powder (195 mg, 80 %). ^{1}H NMR (300 MHz, $CDCl_3$, ppm): 8.31 (d, ^3J = 5.4 Hz, 2H), 7.71 (m, 4H), 7.62 (d, ^3J = 7.8 Hz, 2H), 7.10 (t, ^3J = 7.8 Hz, 2H), 6.94 (t, ^3J = 7.8 Hz, 2H), 6.85 (t, ^3J = 7.8 Hz, 2H), 6.40 (d, ^3J = 7.8 Hz, 2H) 5.57 (s, 1H), 0.90 (s, 18H). ^{13}C NMR (100 MHz, $CDCl_3$, ppm): 194.6, 166.0, 149.1, 148.5, 147.2, 142.2, 137.7, 134.7, 125.9, 124.7, 123.4, 122.6, 118.2, 117.7, 89.8, 41.1, 28.0. MS (ESI) Calcd for $C_{27}H_{35}IrN_2O_2S_2$ 796.1769; Found 796.1775 $[M]^+$.

ii) Other chemical compounds:

The trimethylolpropane triacrylate TMPTA and (3,4-epoxycyclohexane)methyl 3,4-epoxycyclohexylcarboxylate (EPOX or UVACURE 1500) were provided by Allnex (Scheme 4) and used as benchmark monomers for the synthesis of polymer networks through radical and cationic polymerizations, respectively. *N*-vinylcarbazole (NVK), Methyl methacrylate (MMA), *N,N*-Dimethylformamide (DMF), phenacyl bromide (PBr), diphenyliodonium hexafluorophosphate (Ph_2I^+ or Iod), N-Methyldiethanolamine (MDEA) and 2,2,3,3,3-Pentafluoropropyl methacrylate (PmA) were obtained from Aldrich and ethyldimethylaminobenzoate (EDB) from Lamberti Spa ; the compounds were obtained with the highest purity available and used without further purification. MMA and DMF were distilled over calcium hydride prior to use.

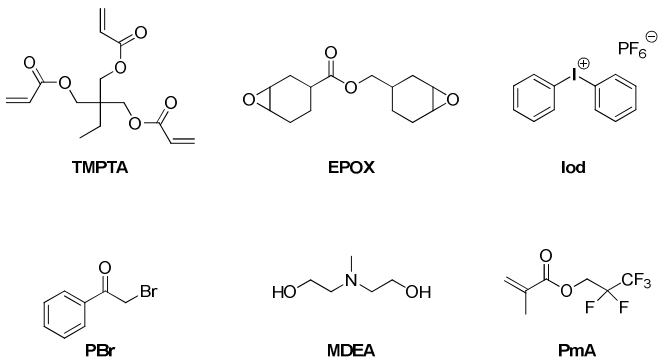

Scheme 4.

iii) Photopolymerization procedures:

In the free radical polymerization, the TMPTA based formulations were irradiated in laminate (the formulations are sandwiched between two polypropylene films). The evolution of the acrylate content is continuously followed by real time FTIR spectroscopy (FTIR NEXUS 870) at ~ 1630 cm^{-1} as presented in [24]. In cationic polymerization, the epoxy based formulations were irradiated under air and the evolution of the epoxy content was followed at ~ 790 cm^{-1}. Halogen lamp, laser diode operating at 457 nm (MBL-III-BFIOPTILAS; $I_0 \approx 100$ mW cm^{-2}), LEDs at 462 nm ($I_0 \approx 10$ mW cm^{-2}) and 405 nm ($I_0 \approx 110$ mW cm^{-2}) were used as irradiation sources.

iv) Photopolymerization in solution

In a typical experiment, nIr: 6 mg, 7.5 mmol, PBr: 0.1 g, 0.5 mmol, DMF: 5 g, 68.41 mmol and MMA: 5 g, 49.94 mmol were added in this order into a dried Schlenk tube. The solution was thoroughly deoxygenated by 4 freeze-pump-thaw cycles. The flask was filled with nitrogen gas and irradiated upon a LED bulb exposure at λ_{max} = 462 nm under magnetic stirring. Molecular weights and conversions were determined by SEC and 1H NMR, respectively.

v) ESR experiments:

ESR spin-trapping (ESR-ST) experiments were carried out using a X-Band EMX-plus spectrometer (Bruker Biospin). The radicals were produced at RT upon a laser diode exposure (457 nm) and trapped by phenyl-*N*-t-butylnitrone (PBN) according to a procedure described in detail in [26].

vi) Redox potentials:

The oxidation potential (E_{ox}) was measured in acetonitrile by cyclic voltammetry with tetrabutyl-ammonium hexafluorophosphate (98%) as a supporting electrolyte (Voltalab 6 Radiometer; the working electrode was a platinum disk and the reference was a saturated calomel electrode-SCE). Ferrocene was used as a standard and the potential determined from the half peak potential. Free energy changes ΔG were calculated according to the Rehm-Weller equation where E_{ox}, E_{red}, E_T, and C are the oxidation potential of the studied iridium complexes, the reduction potential of Iod or phenacyl bromide, the excited triplet state energy of the studied iridium derivatives, and the electrostatic interaction energy for the initially formed ion pair, generally considered as negligible in polar solvents.[27]

$$\Delta G = E_{ox} - E_{red} - E_T + C \qquad \text{(eq. 1)}$$

vii) Fluorescence Experiments:

The steady state fluorescence properties of the different iridium were studied using a JASCO FP-750 spectrometer.

viii) Laser flash photolysis:

Nanosecond laser flash photolysis (LFP) experiments were carried out for the determination of the luminescence lifetimes. The experimental set-up is based on a Q-switched nanosecond Nd/YAG laser (λ_{exc} = 355 nm, 9 ns pulses; energy reduced down to 10 mJ) from Continuum (Minilite) and an analyzing system consisting of a ceramic Xenon lamp, a monochromator, a fast photomultiplier and a transient digitizer (Luzchem LFP 212).[28]

ix) Nuclear Magnetic Resonance (NMR) spectroscopy:

^{1}H NMR spectra were recorded using a Bruker Advance 400 (400.17 MHz) in CDCl3 at 298K.

x) Size Exclusion Chromatography (SEC):

Molecular weights were determined by Size Exclusion Chromatography (SEC) in THF. Solutions of samples with a concentration of around 5.00 mg/mL were prepared and filtered (PTFE membrane; 0.20 µm) before injection. The flow rate was 1.0 mL/min (35°C). The following Agilent 1260 Infinity series setup was used: a G1310B isocratic pump; a G1322A degasser; a G1329B auto-sampler; a G1316A thermostated column compartment equipped

with set of Polymer Laboratories ResiPore columns (nominal particle size: 3 µm; porosity: 2 µm) composed of a guard column (50×7.5 mm) and two columns (300×7.5 mm); a G1314B variable wavelength detector; a G7800A multidetector suite equipped with a MDS refractive index detector and a MDS viscosimeter detector. Universal calibration was performed using a set of EasiVial polystyrene PS-M standards. Agilent GPC/SEC software and multi-detector upgrade were used to determine molar masses values and distributions.

xi) XPS analysis:

X-ray photoelectron spectroscopy (XPS) spectra were recorded with a VG SCIENTA SES-2002 spectrometer equipped with a concentric hemispherical analyzer. The incident radiation used was generated by a monochromatic Al Ká x-ray source (1486.6eV) operating at 420 W (14kV; 30mA). Photo-emitted electrons were collected at a take-off angle of 90° from the surface substrate, with electron detection in the constant analyser energy mode (FAT). Widescan spectrum signal was recorded with a pass energy of 500 eV; for the high resolution spectra (C1s, F1s, O1s, Ir4f, Br3d and N1s), the pass energy was set to 100 eV. The analysed surface area was approximately 3 mm^2 and the base pressure in the analysis chamber during the experiment was about 10^{-9} mbar. Charging effects on these isolating samples were compensated by using of a Flood Gun. The spectrometer energy scale was calibrated using the Ag $3d^{5/2}$, Au $4f^{7/2}$ and Cu $2p^{3/2}$ core level peaks, set respectively at binding energies of 368.2, 84.0 and 932.6 eV. Spectra were subjected to a Shirley baseline and peak fitting was made with mixed Gaussian-Lorentzian components with equal full-width-at-half-maximum (FWHM) using CASAXPS version 2.3.17software. The surface composition expressed in atom% was determined using integrated peak areas of each component and took into account the transmission factor of the spectrometer, the mean free path and the Scofield sensitivity factors of each atom. All the binding energies (BE) are referenced to the aliphatic carbon C1s -(CH_x)- at 285.0 eV and given with a precision of 0.1eV.

xii) Laser direct writing:

Sample preparation: The first polymer layer was prepared from a drop of TMPTA solution containing 0.5w% nIr, 3w% RBr and 5w% MDEA, deposited on a microscope cover slip. The curing was led with a Halogen lamp during 120 sec under laminated conditions at room temperature. After, a second monomer was deposited on top of this film and was irradiated by laser direct-write, the unreacted monomer was washed away by rinsing the surface with ethanol.

Laser direct-write micropatterning: Laser source was a Nd:Yag microlaser emitting at 532 nm (0.6 ns) equiped with an objective x40 (NA=0.65) microscope objective. The beam was injected into an inverted microscope (Zeiss Axio Observer D1). A piezoelectrical stage for micropositioning the sample under the laser beam was controlled by a computer. The microscope is equiped with a CCD camera for visualizing the sample.

Structures characterization: Atomic Force Microscopy (AFM) images were recorded with a PicoPlus microscope operating in resonant mode. The probes were commercially available silicon tips with a spring constant of 13-77 N/m and a resonance frequency of 300 kHz (BS-TAP300 Mode tapping provided by Budgetsensors).

Results and discussion:

1) Light absorption and photochemical properties of nIr

The light absorption properties of the novel iridium complex **nIr** are compared to those of $Ir(ppy)_3$ in Figure 1. The **nIr** compound possesses a molar extinction coefficient $\varepsilon_{max} \sim 7100\ M^{-1}cm^{-1}$ at 372 nm but more interestingly is characterized by an enhanced visible light absorption property: $\varepsilon_{max} \sim 5200\ M^{-1}cm^{-1}$ at 476 nm. Clearly, **nIr** exhibits a better absorption for any irradiation at $\lambda > 300$ nm, e.g. at 457 nm, which represents the maximum emission wavelength for the used laser diode, the ε of **$Ir(ppy)_3$** is 1300 $M^{-1}cm^{-1}$ vs. 4600 $M^{-1}cm^{-1}$ for nIr.

The luminescence (i.e. phosphorescence) lifetimes of the iridium complexes determined under nitrogen are 4.4 μs for **nIr** vs. 1.3 μs for **$Ir(ppy)_3$**. The oxidation potentials of **nIr** and **$Ir(ppy)_3$** as well as the free energy changes ΔG for the oxidation of **nIr** and **$Ir(ppy)_3$** by the phenacyl bromide (ΔG_{PBr}) or the iodonium salt (ΔG_{Iod}) are gathered in Table 1. The ΔGs are all highly favourable ($\Delta G << 0$) suggesting efficient oxidation processes of triplet state of nIr by both PBr and Iod.

Figure 1. UV-visible absorption spectra in acetonitrile **(1)** $Ir(ppy)_3$ and **(2)** nIr.

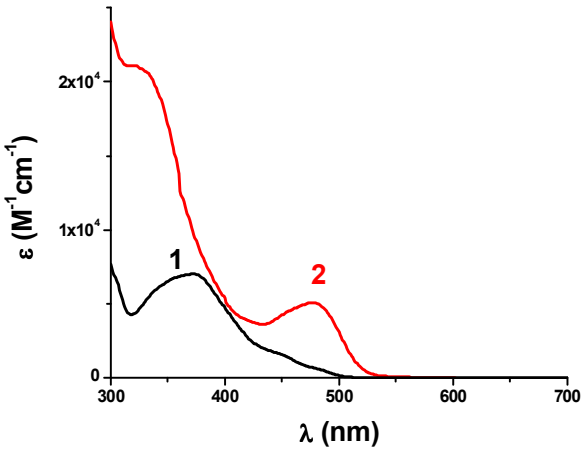

Table 1. Properties of the iridium complexes in acetonitrile: maximum absorption $\lambda_{max\ (abs)}$ and luminescence $\lambda_{max\ (lum)}$ wavelengths, triplet state energy levels (E_T) and luminescence lifetimes (τ), oxidation potentials (E_{ox}) and free energy changes for the oxidation of the triplet states by the phenacyl bromide (ΔG_{PBr}) or the iodonium salt (ΔG_{Iod}).

	$\lambda_{max\ (abs)}$ (nm)	$\lambda_{max\ (lum)}$ (nm)	E_{ox} (V vs SCE)	E_T [b] (eV)	τ (ns)	ΔG_{PBr} [a] (eV)	ΔG_{Iod} [a] (eV)
Ir(ppy)$_3$	372	519	0.77	2.5	1300	-0.95	-1.53
nIr	476	610	0.64	2.25	4400	-0.83	-1.41

a: reduction potentials of -0.2V and -0.78V were used in eq. 1 for Iod and PBr, respectively (from ref [6]).
b: the energy level E_T was determined from the crossing of the absorption and luminescence spectra.

2) Cationic photopolymerization ability of nIr based initiating system

2a/ Polymerization efficiency:

The ring-opening polymerization (ROP) of EPOX was carried out under air upon exposure to different irradiation sources. Interestingly, the **nIr**/Iod system leads to an excellent polymerization profile as shown in Figure 2 curve 1: final conversion ~55% at t = 400 s of irradiation (457 nm laser diode exposure), similar results were obtained upon the halogen lamp. Upon the laser diode at 532 nm, a slightly lower final conversion (~ 40%) is reached (Figure 2, curve 2), resulting from a lower absorption of **nIr**. No polymerization is observed when using Iod and **nIr** alone. Obviously, Ir(ppy)$_3$ does not work at 532 nm (no absorption at this latter wavelength).

The presence of *N*-vinylcarbazole NVK significantly improves the polymerization profiles (Figure 3) e.g. when using the **nIr**/Iod/NVK three-component system at 532 nm, a slightly higher final conversion is obtained (50% vs. 45% with **nIr**/Iod).

Figure 2. Polymerization profiles of EPOX under different irradiation devices using **nIr**/Iod (1%/2% w/w): (1) laser diode 457 nm; (2) laser diode 532 nm; (3) halogen lamp; under air.

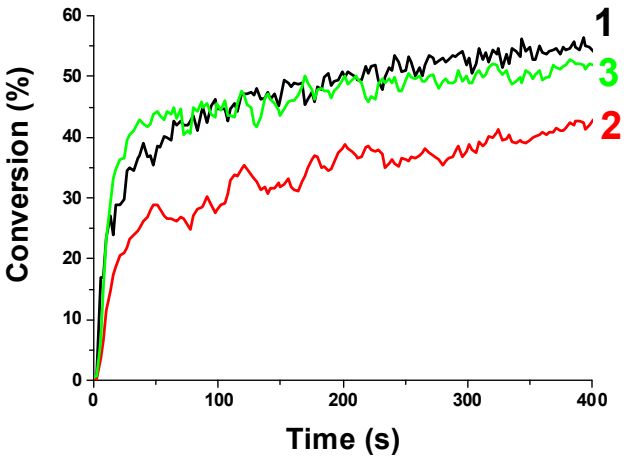

Figure 3. (A) Polymerization profiles of EPOX using different photoinitiating systems: (1) nIr/Iod (1%/2% w/w); (2) nIr/Iod/NVK (1%/2%/3% w/w); **(B)** conversion of the NVK double bond for (2). Laser diode irradiation at λ = 532 nm; under air.

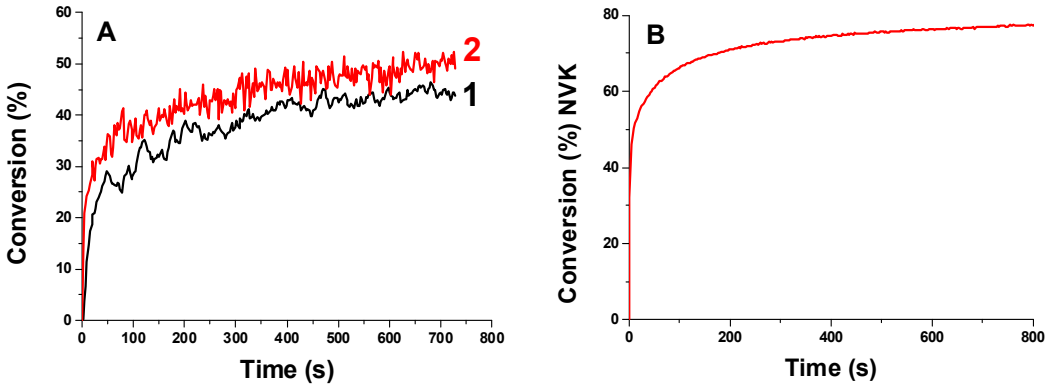

2b/ Chemical mechanisms:

A strong quenching of the luminescent excited state (^{3}**nIr**) by Iod at 610 nm is observed in Figure 4. The interaction rate constant calculated from a Stern-Volmer treatment (k_q ~ 7.4

10^9 $M^{-1}s^{-1}$) is close to the diffusion limit and underlines a very fast process in agreement with its associated negative ΔG (see above and Table 1).

The **nIr**/Iod interaction corresponds to an efficient electron transfer process that promotes the decomposition of the iodonium salt (r1b). Indeed, phenyl radicals $Ph^{\bullet}$ are detected by ESR spin-trapping experiments (using phenyl-N-*t*-butylnitrone PBN as a spin trap) during the irradiation of the **nIr**/Iod couple at 457 nm (Figure 5). The *hfc* constants are: $a_N \sim 14.2$ G; $a_H \sim 2.2$ G in agreement with the known data for this PBN adduct.[23a] In the same conditions, **nIr** or Iod alone don't generate any free radical upon visible light.

In Figure 6, the steady state photolysis of the **nIr**/Iod solution (under the halogen lamp) clearly shows the consumption of **nIr** in line with reaction r1b.

In the presence of NVK, $Ph^{\bullet}$ is converted into a Ph-$NVK^{\bullet}$ radical through its addition to the NVK double bond (r2a). Ph-$NVK^{\bullet}$ is an electron rich radical, easily oxidizable by $\mathbf{nIr}^{IV}$ or Iod to form a Ph-NVK^{+} cation (r2b, r2c; it has been already shown [29] that such a cation is a powerful structure to initiate the cationic polymerization of EPOX). Moreover, the **nIr** ground state is recovered in r2b in agreement with a photocatalyst behavior.

$$nIr \rightarrow {}^1nIr \quad (h\nu) \quad \text{and} \quad {}^1nIr \rightarrow {}^3nIr \qquad \text{(r1a)}$$

$${}^3nIr + Ph_2I^+ \rightarrow nIr^{IV} + PhI + Ph^{\bullet} \qquad \text{(r1b)}$$

$$Ph^{\bullet} + NVK \rightarrow Ph\text{-}NVK^{\bullet} \qquad \text{(r2a)}$$

$$Ph\text{-}NVK^{\bullet} + nIr^{IV} \rightarrow Ph\text{-}NVK^{+} + nIr \qquad \text{(r2b)}$$

$$Ph\text{-}NVK^{\bullet} + Ph_2I^+ \rightarrow Ph\text{-}NVK^{+} + PhI + Ph^{\bullet} \qquad \text{(r2c)}$$

Figure 4. Luminescence quenching of ^{3}nIr by Iod in acetonitrile; $[Ph_2I^+]$ = 0 M; 0.0032 M; 0.0086 M, respectively.

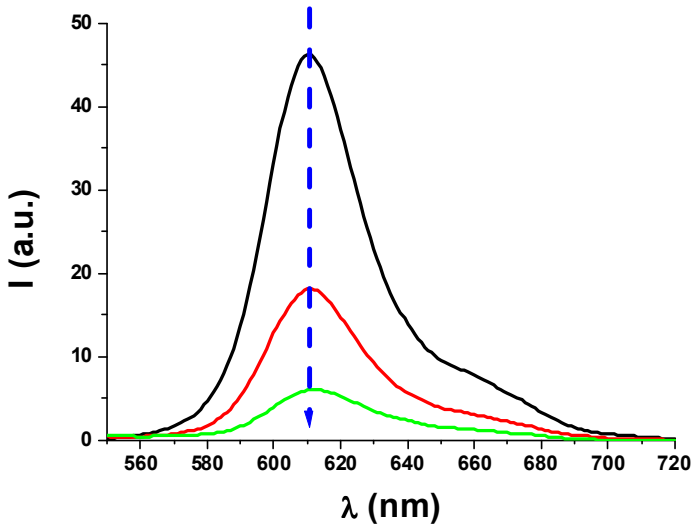

Figure 5. ESR spectra obtained upon irradiation of **nIr**/Iod in *tert*-butyl-benzene: (a) experimental and (b) simulated ESR spectra. Phenyl-N-*t*-butylnitrone (PBN) is used as a spin trap; laser diode exposure at λ = 457 nm.

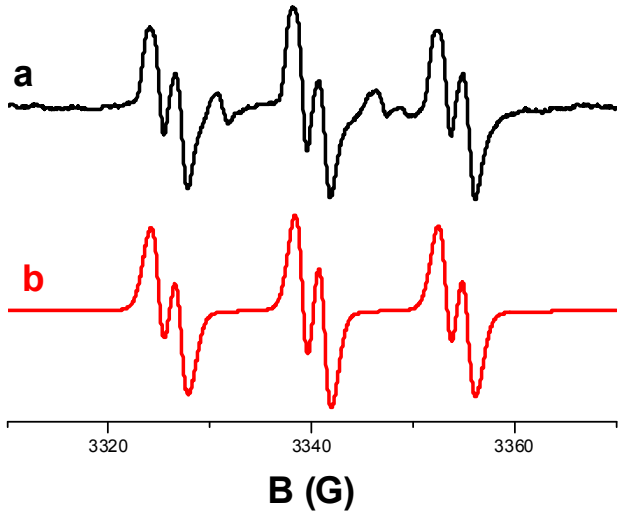

Figure 6. Photolysis of the **nIr**/Iod couple; upon halogen lamp irradiation (from t = 0 to 20 s); in acetonitrile; $[Ph_2I^+]$ = 0.0251 M.

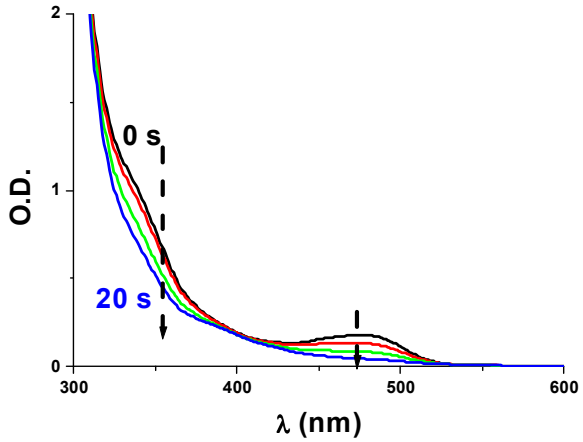

3) Radical polymerization ability of of nIr based initiating system

3-a/ Photopolymerization for the access to acrylate polymer networks

The free radical polymerization FRP of a trifunctional acrylate monomer (TMPTA) in laminate at 457 nm using different photoinitiating systems is represented in Figure 7. **Ir(ppy)$_3$** or **nIr** alone does not work. **Ir(ppy)$_3$**/PBr and **Ir(ppy)$_3$**/PBr/MDEA are totally inefficient (Figure 7 curves 1 and 3). On the opposite, final conversions of ~ 30% and 47% are obtained in the presence of **nIr**/PBr and **nIr**/PBr/MDEA, respectively (Figure 7 curves 3 and 4). The much better efficiency/reactivity of **nIr** can probably be ascribed to its much better light absorption properties at 457 nm.

Figure 7. Polymerization profiles of TMPTA using different photoinitiating systems: (1) Ir(ppy)$_3$/PBr (0.5%/3% w/w); (2) nIr/PBr (0.5%/3% w/w); (3) Ir(ppy)$_3$/PBr/MDEA (0.5%/3%/5% w/w); (4) nIr/PBr/MDEA (0.5%/3%/5% w/w); under the diode laser 457 nm exposure; in laminate.

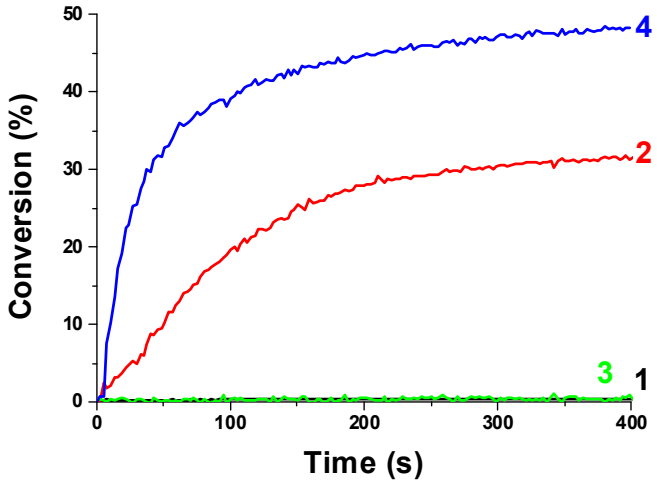

nIr being in-situ embedded in the synthesized network during the photopolymerization, the synthesized polymer exhibits luminescence properties. The luminescence lifetime of nIr in the synthesized polymer has been determined by laser flash photolysis. Interestingly a lifetime of 5 μs has been found in good agreement with the value in solution (4.4 μs). This shows that nIr is not degradated during the photopolymerization in full agreement with its photocatalyst behavior (see below Scheme 5).

3-b/ Towards a photocontrolled polymerization of methacrylates ?

As $Ir(ppy)_3$ has been recently reported as an excellent photocatalyst for photocontrolled polymerization (see in introduction), the ability of **nIr** in such processes deserves to be investigated. Polymerization of methyl methacrylate (MMA) in DMF under nitrogen using the **nIr**/PBr photoinitiating system was carried out upon a LED bulb exposure at λ_{max} = 462 nm (Figure 8). Samples were withdrawn regularly for SEC analysis (the sample was precipitated in methanol, filtered and dried under vacuum). The linearity of $\ln([MMA]_0/[MMA])$ as a function of time, as well as the linear relationship between molecular weights and conversion evidence the control of the polymerization at its beginning. (Figures 8A & 8B). However, the control is obviously progressively lost for longer polymerization times, with polydispersity indexes becoming broader, in particular due to a molar masses distribution becoming bimodal, which reveals a significant fraction of dead chains (Figure 8C).

The control is improved for a lower catalyst concentration, a similar behavior was found in [16a]. Reducing the **nIr** amount to 0.6 mg (0.7 µmol) improves the polydispersity (ranging between 1.4 to 1.6 for conversion < 40%) (Figure 8D); the shoulder for low molecular weight is also not observed for these conditions. However, this control of the polymerization is still not perfect. For a better understanding of this behavior, some photolysis experiments were carried out. Interestingly, a clearly photolysis of nIr alone in DMF is found i.e. an important decrease of the band at 480 nm ascribed to nIr is observed after 15h of irradiation (Figure 9). This suggests that nIr is not perfectly stable upon light irradiation in this solvent. An exchange of ligands or other side reactions can perhaps occur. This consumption of the nIr photocatalyst in the course of the photopolymerization reaction can explain the partial lose of control with the irradiation time.

Figure 8. Polymerization profiles of MMA in DMF using nIr/PBr (**nIr**: 7.5 µmol, PBr: 0.5 mmol, DMF: 68.41 mmol, MMA: 49.94 mmol) upon 462 nm LED bulb irradiation, **(A)** Evolution of $\ln([M]_0/[M])$ as a function of time; **(B)** Evolution of Mn with conversion; **(C)** SEC chromatograms (refractive index detector signals) for polymers obtained with different irradiation times; **(D)** SEC chromatograms (refractive index detector signals) for polymers obtained with different irradiation times for a different concentration in nIr (nIr 0.7 µmol); LED@405 nm irradiation.

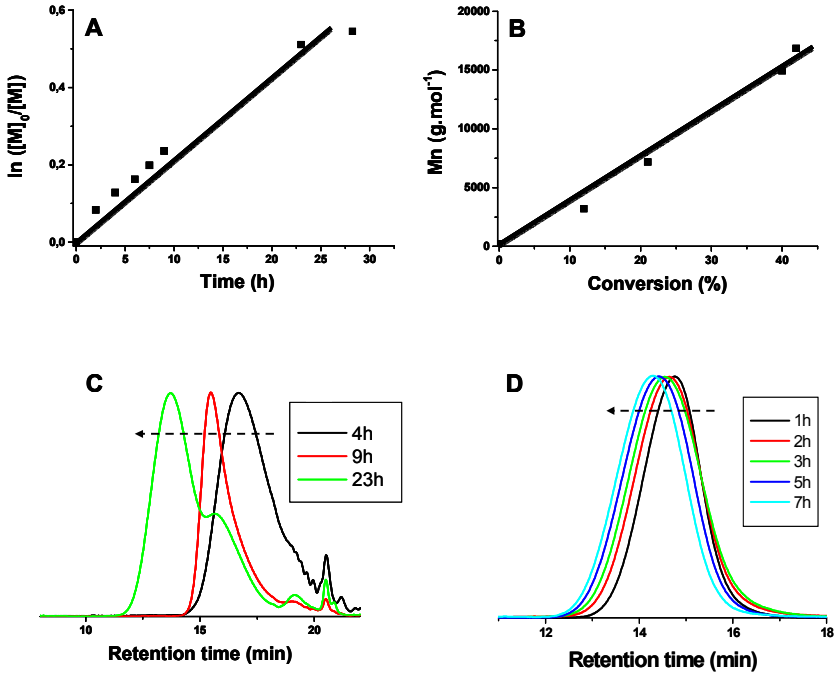

Table 1. Parameters characterizing the polymers synthesized in the given conditions: (A) MMA in DMF using nIr/PBr (**nIr**: 7.5 µmol, PBr: 0.5 mmol, DMF: 68.41 mmol, MMA: 49.94 mmol) upon 462 nm LED bulb irradiation (see Figure 8C for the SEC chromatograms); (B) MMA in DMF using nIr/PBr (**nIr**: 0.7 µmol, ethyl α-bromophenylacetate: 0.5 mmol, DMF: 68.41 mmol, MMA: 49.94 mmol) upon 462 nm LED bulb irradiation (see Figure 2 in SI for the SEC chromatograms).

Conditions	Irradiation time (h)	Conversion (%)	Mn (g/mol)	Mw (g/mol)	Ip
A	4	12	3190	5790	1.8
A	9	21	7170	11980	1.7
A	23	40	14940	67890	4.5
B	3	14	17700	23520	1.3
B	6	26	23590	27550	1.2
B	8.5	49	25140	30560	1.2

To improve the controlled process, a decrease of the catalyst content as well as a change for another initiator were investigated (ethyl α-bromophenylacetate is now used as initiator). A better reactivity of the system is noted with the presence of ethyl α-bromophenylacetate (Table 1) i.e. 40% of conversion after 23 h of irradiation with PBr vs. 49% after 8.5 h with ethyl α-bromophenylacetate. The polydispersity indexes are also improved (1.2-1.3), no shoulder corresponding to the formation of dead chains is observed (see Figure S1 in SI). For this initiator, the linear relationship between molecular weights and conversion also evidences the control of the polymerization.

Figure 9. Photolysis of **nIr** in DMF upon halogen lamp irradiation. Under nitrogen.

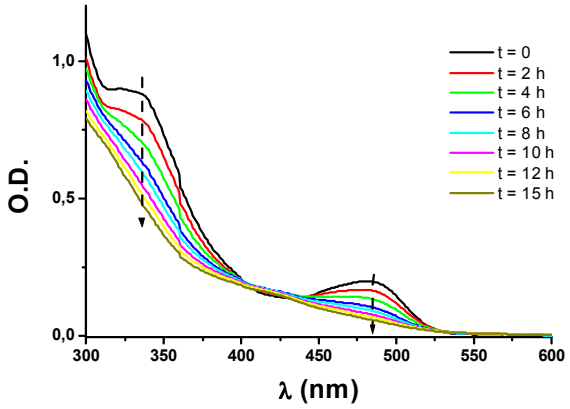

3-c/ Chemical mechanism

In Figure 10, ESR spin trapping experiments show that the **nIr**/PBr interaction leads to phenacyl radicals after irradiation at 457 nm (*hfc*: a_N = 14.4 G and a_H = 4.0 G in agreement with known data for a phenacyl/PBN adduct [24d]). This occurs through reaction (r3); the ΔG for this process has been found favorable in Table 1.

$$^3\text{nIr} + \text{PBr} \rightarrow \text{nIr}^{IV} + \text{PBr}^{\bullet -} \quad \text{and} \quad \text{PBr}^{\bullet -} \rightarrow \text{P}^{\bullet} + \text{Br}^- \qquad \text{(r3)}$$

Figure 10. ESR spectra obtained upon irradiation of **nIr**/PBr in *tert*-butyl-benzene. Phenyl-N-*t*-butylnitrone (PBN) is used as a spin trap; laser diode exposure at λ = 457 nm: (a) experimental and (b) simulated ESR spectra.

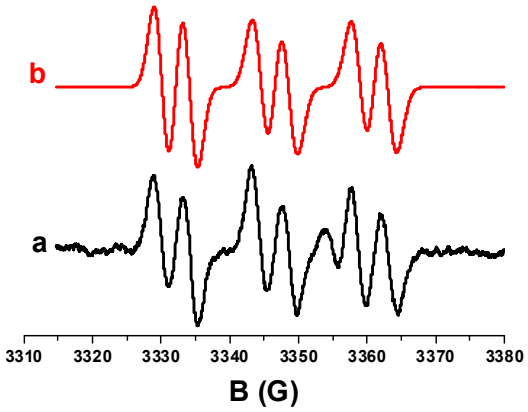

The quenching rate constant of ^{3}**nIr** by PBr is almost diffusion controlled ($k = 2.8 \times 10^{10}$ M^{-1} s^{-1}; luminescence quenching experiments; ΔG = - 0.83 eV) whereas that of ^{3}**nIr** by MDEA is $<< 2 \times 10^8$ M^{-1} s^{-1}. Therefore, **nIr**/PBr two-component system necessarily operates through an oxidation cycle (Scheme 5A). The generated nIr^{III}* (nIr*) is quenched by PBr, ii) the formed nIr^{IV}Br (formally written $\text{nIr}^{\bullet +}/\text{Br}^-$) is reduced by the radicals leading to a regeneration of **nIr**. In the same way, the particular **nIr**/PBr/MDEA three-component system used here also operates according to a similar oxidative catalytic cycle where reaction (r4) is added (see Scheme 5B for the comparison of the two-component vs. three-component systems): this is rather unexpected as a reduction cycle is usually considered in other iridium complex/alkyl halide/amine systems proposed in the literature [see in 11]. A reduction cycle

seems also appropriate in some reported iridium complex/PBr/MDEA systems.[24d] The better efficiency of **nIr**/PBr/MDEA in the FRP of TMPTA vs. **nIr**/PBr likely results from the additional $MDEA_{-H}^{\bullet}$ aminoalkyl initiating radicals produced in (r5).

$$nIr^{IV} + MDEA \rightarrow nIr + MDEA^{\bullet+} \quad (r4)$$

$$MDEA^{\bullet+} \rightarrow H^{+} + MDEA_{(-H)}^{\bullet} \quad (r5)$$

As suggested in [16a] and confirmed above, the possible living character of the FRP in both the two- and three-component system can be explained on the basis of additional reactions involving the reduction of nIr^{IV} by any $PM_n^{\bullet}$ growing acrylate macroradical and the oxidation of nIr^{III*} by any PM_n-Br polymer chains (Scheme 5). Thus, a dormant PM_n-Br polymer is formed.

Scheme 5. Comparison of the catalytic cycles for the two-component nIr/PBr (A) and the three-component nIr/PBr/amine (B) systems.

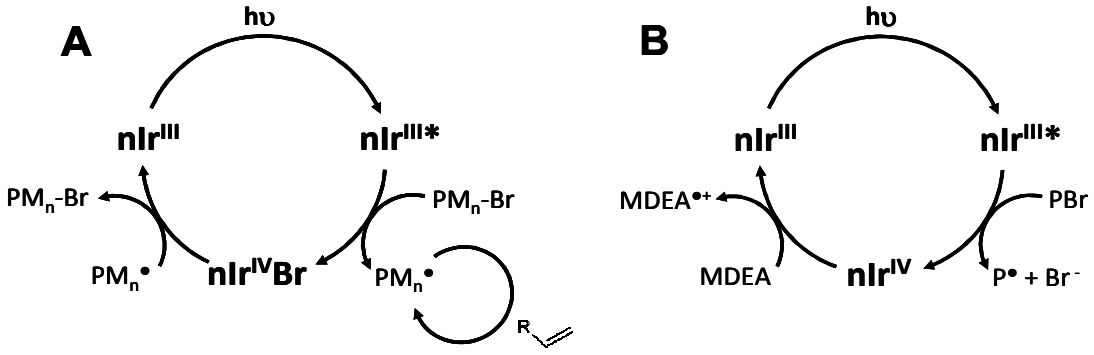

4) The nIr/PBr/MDEA three-component photoinitiating system for polymer surface modification

The dormant PM_nBr species formed in Scheme 5 should be a good candidate for a further re-initiation of the polymerization. In Figure 11, it can be observed that for the nIr/PBr/MDEA system, the polymerization only occurs in presence of light i.e. the polymerization stops when the light is switched off and restarts when the light is switched on. Similar "on/off" polymerization profiles were obtained for $Ir(ppy)_3$/PBr in [16a].

Figure 11. Polymerization profile for TMPTA upon a laser diode@457 nm (in laminate) for the initiating system nIr/PBr/MDEA (0.5%/3%/5% w/w).

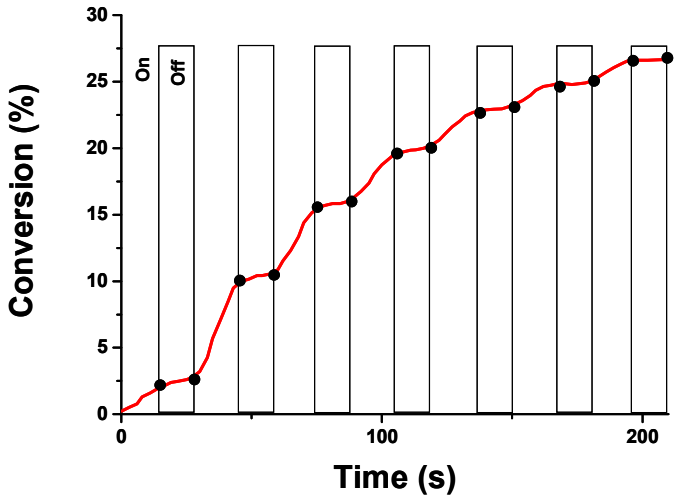

These re-initiation properties can be highly worthwhile for surface modifications and synthesis of covalently bounded multilayer materials. Here, a first polyacrylate layer is synthesized using the **nIr**/PBr/MDEA photoinitiating system as before (Figure 12) i.e. the TMPTA formulation is deposited on a glass slide and irradiated for 5 minutes with a halogen lamp, in laminate. A contact angle (polymer/water) of 40° is measured, showing a hydrophilic character of the surface. The surface is washed with acetone to remove the unreacted monomer. Then a fluoro-monomer (PmA) is poured on the first layer and irradiated (5 mn; halogen lamp). The contact angle of this second polymerized layer is now 110° in line with the hydrophobicity of the fluorinated polymer. This result highlights the very good re-initiation ability of the **nIr**/PMnBr system present in the first layer.

The re-initation of the second layer is also fully supported by an XPS analysis. This latter technique gives information about the outermost surface of the sample in a 6-9 nm range. On the wide scan of the top of the second layer, only carbon, fluorine, oxygen, and weak traces of nitrogen and bromine are detected. The elementary atomic percentages of each species are gathered in Table 2. Figure 13 highlights the presence of fluorine in the F1s and C1s high resolution XPS spectra. The low concentration of iridium used to initiate the radical

photopolymerization is detected by XPS in the first layer (Figure14). Bromine and nitrogen (coming from PBr and MDEA, respectively) are also detected.

Figure 12. Contact angles of **(A)** the polymerized TMPTA first layer using nIr/PBr/MDEA (0.5%/3%/5% w/w) and **(B)** the polymerized fluoromonomer (PmA) second layer after re-initiation. Halogen lamp irradiation

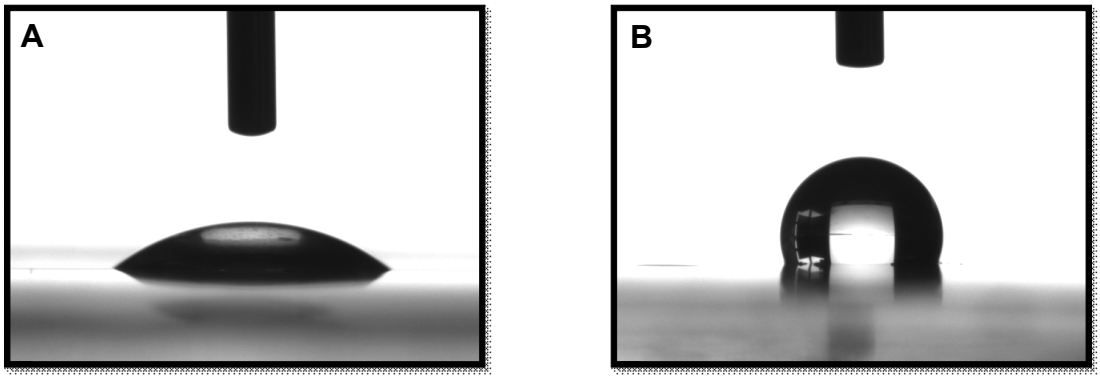

Table 2: Quantification of the compounds present on the top of the second polymer layer.

Br 3d %	C 1s %	F 1s %	N 1s %	O 1s %
0,08	62,67	20,67	0,85	15,71

Figure 13. F1s (left) and C1s (right) high resolution XPS spectra after re-initiation and formation of the fluorinated polymer.

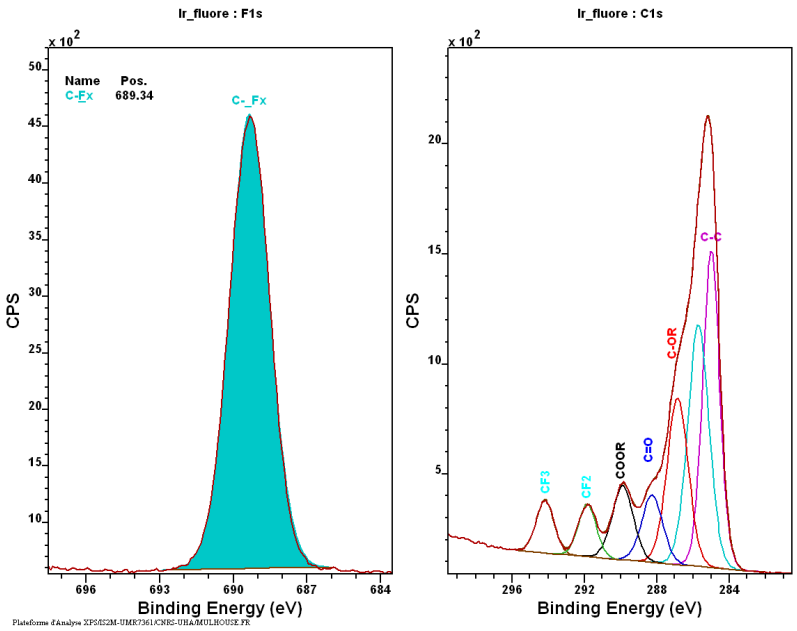

Figure 14. High resolution XPS spectrum of the iridium-bromine region for the first layer.

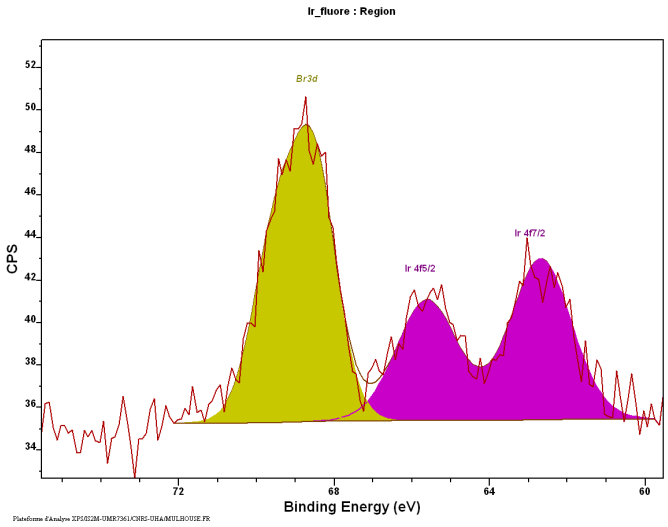

Using the chemical mechanisms observed for **nIr**, this approach for surface modifications has been also extended to other iridium based complexes (Scheme 1 in SI). These latter compounds were also characterized by excellent visible light absorption properties (Figure 2 in SI). As observed for nIr, these Iridium complexes can also be used for surface modifications (Figure 3 in SI).

5) The photoredox catalysis with nIr/PBr/MDEA system for laser direct writing

Extending the absorption spectrum of the photoiniator system towards visible wavelengths opens the possibility to use visible laser for direct write. Such technique is very interesting for generating arbitrary microstructures. Recourse to visible light sources significantly simplifies the implementation from optics point of view. This possibility was demonstrated using a green Nd:YAg microlaser emitting at 532 nm. The main results are plotted in Figure 15. A first set of experiments (Figure 15a) was used to determine and optimize the photonic conditions for generating micropatterns with controlled height. The laser power was varied for a constant irradiation time (5 ms) and height was measured by AFM. A threshold power of 20 µW was observed. Under such value, the concentration of radicals formed is too low to efficiently start the free radical polymerization, due to oxygen inhibition. Then, when the power is increased, an increase of the line height was observed.

Interestingly, a simple parameter like laser power can be used to tune the patterns heights. Remarkably, the pattern height could be tuned from nm to microscale with very good accuracy.

The main advantage of laser direct write on mask lithography techniques is to open the possibility to generate arbitrary structures thanks to the control of the laser displacement over the sample surface. To exemplify this point and stress out the potential of the technique, regular grids (Figure 15b) and a logo (Figure 15c) were generated by repolymerization on the polymer surface. In both cases, it was observed that the height of the structure is maintained constant for the whole structure, demonstrating that the control of the spatial extend of the polymerization reaction is efficient using this molecular system. One major difference of our approach is to guarantee a covalent linking of the micropatterns to the primary polymer surface. Moreover, any acrylate formulation can be used for repolymerization.

Figure 15. Laser direct-write using a Nd:Yag microlaser (532 nm, 0.6 ns) with X40 microscope objective. a) Control of line height with laser power for 5 ms irradiation (3D image in inset). AFM images of complex microstructures: b) grid created with 800 µW, 5 ms (3D image and cross-section) and c) logo created with 130 µW, 10 ms .

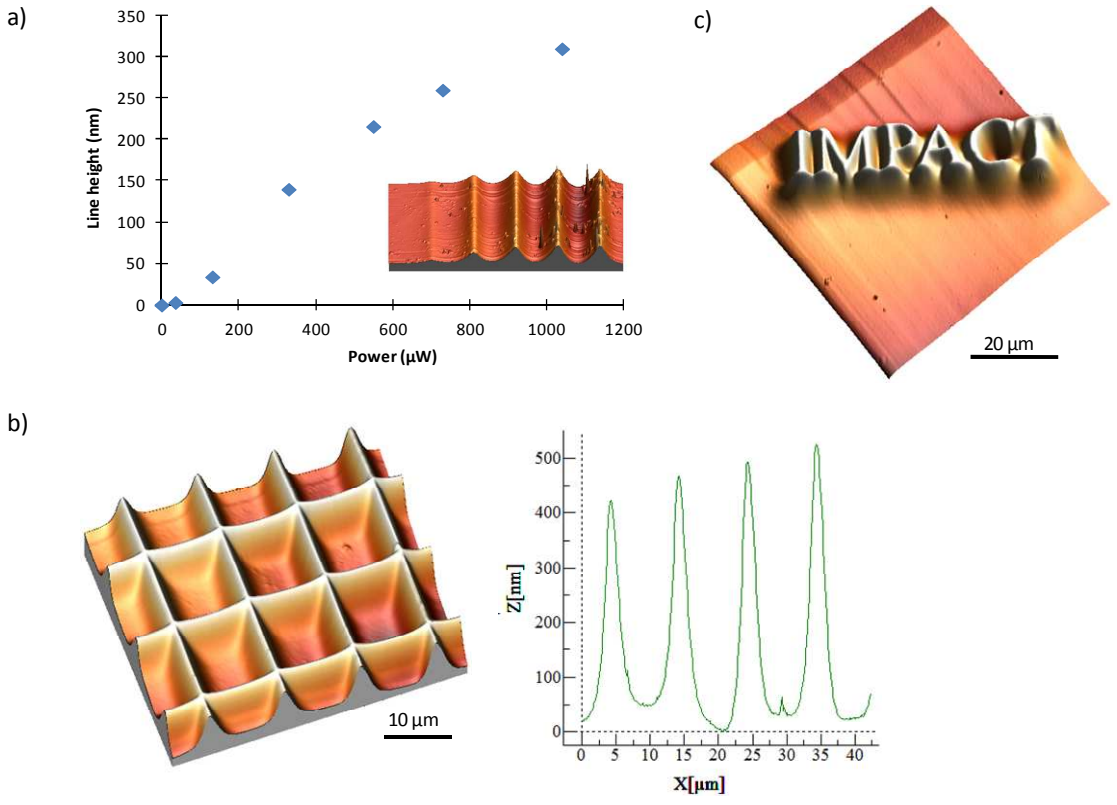

Conclusion:

This paper shows that radical and cationic polymerization reactions can be initiated under 457 to 532 nm lights by a photoinitiating system PIS containing a newly designed iridium complex (**nIr**). A photocatalytic behavior of these PISs are noted. A striking result is the working out of the **nIr**/PBr/MDEA system through an unexpected oxidative cycle: this might be the first known example of such a cycle in a Ir complex/PBr/amine combination. This **nIr** sample can also be useful in controlled photopolymerization at 462 nm i.e. an increase of the molecular weight vs. conversion is found. Re-initiation experiments under light allow easy surface modifications by grafting a polymerizable top layer. Laser direct writing experiments can also be easily carried out. To our opinion, there is still a place to design other high-performance iridium complexes in term of light absorption and reactivity.

Acknowledgements: The authors thank the *Agence Nationale de la Recherche* for the grant IMPACT. The authors thank Dr. Didier Le Nouen (ENSCMu) for the help in NMR experiments.

References:

[1] a) Nicewicz, D.A.; MacMillan, D.W.C. *Science.* **2008**, 322, 77-80; b) Nagib, D.A.; Scott, M.E.; MacMillan, D.W.C. *J. Am. Chem. Soc.* **2009**, 131, 10875-10877; c) Shih, H-W.; Vander Wal, M.N.; Grange, R.L.; MacMillan, D.W.C. *J. Am. Chem. Soc.* **2010**, 132, 13600-13603.

[2] a) Narayanam, J.M.R.; Stephenson, C.R.J. *Chem. Soc. Rev.* **2011**, 40, 102-113; b) Dai, C.; Narayanam, J.M.R.; Stephenson, C.R.J. *Nature Chem*. **2011**, 3, 140-145; c) Nguyen, J.D.; Tucker, J.W.; Konieczynska, M.D.; Stephenson, C.R.J. *J. Am. Chem. Soc*. **2011**, 133, 4160-4163.

[3] a) Ischay, M.A.; Lu, Z.; Yoon, T.P. *J. Am. Chem. Soc.* **2010**, 132, 8572-8574; b) Du, J.; Yoon, T.P. *J. Am. Chem. Soc.* **2009**, 131, 14604-14605; c) Yoon, T.P.; Ischay, M.A.; Du, J. *Nature Chem.* **2010**, 2, 527-532.

[4] a) Larraufie, M.H.; Pellet, R.; Fensterbank, L.; Goddard, J.P.; Lacôte, E.; Malacria, M.; Ollivier, C. *Angew. Chem. Int. Ed.* **2011**, 50, 4463-4466; b) Courant, T.; Masson, G.; *Chem. Eur. J.* **2012**, 18, 423-427; c) Baralle, A.; Fensterbank, L.; Goddard, J.P.; Ollivier, C. *Chem. Eur. J.* **2013**, 19, 10809-20813.

[5] a) Neumann, M.; Fuldner, S.; Konig, B.; Zeitler, K. *Angew. Chem. Int. Ed.* **2011**, *50*, 951-954; b) Zeitler, K. *Angew. Chem. Int. Ed.* **2009**, 48, 9785-9789.

[6] Fouassier, J.P.; Lalevée, J.; *Photoinitiators for Polymer Synthesis: Scope, Reactivity and Efficiency*, Wiley-VCH., Weinheim, **2012**.

[7] a) Belfied, K.D.; Crivello, J.V. *Photoinitiated Polymerization.* Washington DC: ACS Symposium series 847; **2003**; b) *Photochemistry and UV Curing*, Fouassier, J.P. Ed., Research Signpost, Trivandrum India, **2006**; c) *Handbook of Vinyl Polymers*, Mishra, M.K.; Yagci, Y. Eds., CRC Press, Boca Raton, **2009**; d) Dietliker K. A *Compilation of Photoinitiators commercially available for UV today*, Edinburgh, London: Sita Technology Ltd; **2002**; e) Crivello JV. *Photoinitiators for Free Radical, Cationic and Anionic Photopolymerization*, 2nd edition: John Wiley & Sons: Chichester; **1998**; f) Cunningham Jr, A.F.; Desobry, V. in *Radiation Curing in Polymer Science and Technology*, Fouassier J.P., Rabek, J.F., Eds., Elsevier Science Publishers LTD, London, **1993**, vol. 2, 323-374; g) Kunding, E.P., Xu, L.H., Kondratenko, M., Cunningham, A.F. Jr., Kuntz, M., *Eur. J. lnorg. Chem*. **2007**, 161, 2934-2943.

[8] Lalevée, J.; Blanchard, N.; Tehfe, M.A.; Chany, A.C.; Morlet-Savary, F.; Fouassier, J.P.; *Macromolecules*. **2010**, 43, 10191-10195.

[9] Tehfe, M.A.; Lalevée, J.; Morlet-Savary, F.; Blanchard, N.; Graff, B.; Fouassier,.J.P.; *Macromolecules*. **2012**, 45, 1746-1752.

[10] Zhang, G.; Song, I.Y.; Ahn, K.H.; Park, T.; Choi, W. *Macromolecules*. **2011**, 44, 7594-7599.

[11] Lalevée, J.; Telitel, S.; Xiao, P.; Lepeltier, M. ; Dumur, F.; Morlet-Savary, F.; Gigmes, D.; Fouassier, J.P.; *Beilstein J. Org. Chem.* **2014,** 10*,* 863-876.

[12] a) Matyjaszewski, K., in ACS symposium series, *Advances in Controlled/Living Radical Polymerization,* **2002,** American Chemical Society. b) Matyjaszewski, K., in ACS symposium series, *Controlled Radical Polymerization*, **1998**, American Chemical Society.

[13] Konkolewicz , D.; Schröder , K.; Buback , J.; Bernhard , S.; Matyjaszewski, K. *ACS Macro Lett.* **2012**, 1, 1219–1223

[14] Tasdelen, M. A.; Ciftci, M.; Yagci, Y. *Macromol. Chem. Phys.* **2012**, 213, 1391–1396

[15] Zhang, T. ; Chen, T. ; Amin, I. ; Jordan, R. *Polym. Chem.* **2014**, DOI: 10.1039/C4PY00346B.

[16] a) Fors, B. P.; Hawker, C. J. *Angew. Chem. Int. Ed*. **2012**, 51, 8850-8853; b) Treat, N. J.; Fors, B. P.; Kramer, J. W.; Christianson, M.; Chiu, C-Y.; Read de Alaniz, J.; Hawker, C. J. *ACS Macro Lett.* **2014**, 3, 580–584.

[17] a) Xu, J.; Jung, K.; Atme, A.; Shanmugam, S.; Boyer, C. *J. Am. Chem. Soc.* **2014**, 136, 5508–5519; b) Xu, J.; Atme, A.; Marques Martins, A.F.; Jung, K.; Boyer, C. *Polym. Chem.* **2014**, 5, 3321-3325.

[18] Mosnáček, J.; Ilčíková, M. *Macromolecules.* **2012**, 45, 5859-5865.

[19] a) Zhang, X.; Zhao, C.; Ma, Y.; Chen, H.; Yang, W. *Macromol. Chem. Phys.* **2013**, 214, 2624-2631; b) Ma, W.; Chen, H.; Ma, Y.; Zhao, C.; Yang, W. *Macromol. Chem. Phys.* **2014**, 215, 1012-1021.

[20] Ohtsuki, A.; Goto, A.; Kaji, H. *Macromolecules.* **2013**, 46, 96-102.

[21] Yamago, S.; Nakamura, Y.; *Polymer*. **2013**, 54, 981-994.

[22] Guillaneuf, Y. ; Bertin, D. ; Gigmes, D. ; Versace, D.-L. ; Lalevée, J. ; Fouassier, J. P. *Macromolecules.* **2010**, 43, 2204-2212.

[23] a) Lalevée, J.; Blanchard, N.; Tehfe, M.A.; Morlet-Savary, F.; Fouassier, J.P. *Macromolecules.* **2010**, 43, 10191-10195 ; b) Lalevée, J.; Blanchard, N.; Tehfe, M.A.; Peter, M.; Morlet-Savary, F.; Fouassier, J.P. *Macromol. Rapid Comm.* **2011**, 32, 917-920 ; c)

Lalevée, J.; Blanchard, N.; Tehfe, M.A.; Peter, M.; Morlet-Savary, F.; Gigmes, D.; Fouassier, J.P. *Polym. Chem.* **2011**, 2, 1986-1991.

[24] a) Lalevée, J.; Blanchard, N.; Tehfe, M.A.; Peter, M.; Morlet-Savary, F.; Fouassier, J.P. *Polym. Bull.* **2012**, 68, 341-347; b) Lalevée, J.; Peter, M.; Dumur, F.; Gigmes, D.; Blanchard, N.; Tehfe, M.A.; Morlet-Savary, F.; Fouassier, J.P. *Chem. Eur. J.* **2011**, 17, 15027-15031; c) Lalevée, J.; Tehfe, M.A.; Morlet-Savary, F.; Graff, B.; Dumur, F.; Gigmes, D.; Blanchard, N.; Fouassier, J.P.; *Chimia*, **2012**, 66, 439-441; d) Lalevée, J.; Tehfe, M.A.; Dumur, F.; Gigmes, D.; Blanchard, N.; Morlet-Savary, F.; Fouassier, J.P. *ACS Macro Lett*. **2012**, 1, 286-290.

[25] a) Amarne, H.; Baik, C.; Murphy, S. K.; Wang, S. Chem. Eur. J. 2010, 16, 4750−4761; b) M. Nonoyama, Bull. Chem. Soc. Jpn. 47 (**1974**) 767; H. Woo, S. Cho, Y. Han, W.-S. Chae, D.-R. Ahn, Y. You, W. Nam, J. Am. Chem. Soc. **2013**, 135, 4771−4787.

[26] a) Tordo, P. *Spin-trapping: recent developments and applications*. In: Atherton, N.M., Davies, M.J., Gilbert, B.C., eds., Electron Spin Resonance, volume 16. Cambridge, The Royal Society of Chemistry; **1998**; b) Lalevée, J.; Dumur, F.; Mayer, C.R.; Gigmes, D.; Nasr, G.; Tehfe, M.A.; Telitel, S.; Morlet-Savary, F.; Graff, B.; Fouassier, J.P. *Macromolecules.* **2012**, 45, 4134–4141.

[27] Rehm, D.; Weller, A. *Isr. J. Chem.* **1970**, 8, 259-271.

[28] Lalevée, J.; Telitel, S.; Tehfe, M-A.; Fouassier, J-P.; Curran, D.P.; Lacôte, E. *Angew. Chem. Int. Ed.* **2012**, 51, 5958-5961.

[29] a) Hua Y., Crivello J.V., J. Polym. Sci. A: Polym. Chem. **2000**, 38, 3697-3709; b) Lalevée J., Tehfe M-A., Zein-Fakih A., Ball B., Telitel S., Morlet-Savary F., Graff B., Fouassier J-P., ACS Macro Lett. **2012**, 1, 802-806.

TOC Graphic: